JOURNAL OF Materials CHEMISTRY

Exfoliation of layered perovskite, $KCa_2Nb_3O_{10}$, into colloidal nanosheets by a novel chemical process

Yang-Su Han, In Park and Jin-Ho Choy*

National Nanohybrid Materials Laboratory, School of Chemistry and Molecular Engineering, College of Natural Sciences, Seoul National University, Seoul 151-747, Korea. E-mail: jhchoy@plaza.snu.ac.kr

Received 26th July 2000, Accepted 20th November 2000
First published as an Advance Article on the web 15th February 2001

A novel chemical exfoliation of perovskite-like $KCa_2Nb_3O_{10}$ utilising an amino acid intermediate is described. At first, amino acid intercalated layered perovskite is prepared by ion-exchange reaction between the interlayer protons in $HCa_2Nb_3O_{10}$ and cationic aminoundecanoic acid ($H_3N^+(CH_2)_{10}COOH$; AUA) under an acidic aqueous solution (pH *ca.* 3). Upon intercalation, the basal spacing of $HCa_2Nb_3O_{10}$ expands from 14.7 Å to 30.4 Å to form a paraffin-like monolayer arrangement of interlayered AUA molecules between the perovskite slabs. Subsequent infinite expansion of the oxide layers, which eventually leads to the exfoliation of perovskite slabs ($Ca_2Nb_3O_{10}$) into elementary oxide nanosheets, is accomplished by a host–guest repulsive interaction induced by deprotonation of the carboxylic groups in the interlayered amino acid molecules with NaOH titration. This argument is supported by a gradual decrease in the X-ray intensities of (00*l*) reflections upon base titration. The base titration curve and the zeta (ζ) potential measurement as a function of pH suggest that the intralayer deprotonation of carboxylic groups occurs rapidly in the pH range 8–9. A significant spectral blue shift for the colloidal particles compared to the pristine $HCa_2Nb_3O_{10}$ in the UV-vis absorption spectra also substantiates the delamination of bulk oxide layers into individual monolayers. Atomic force microscopy (AFM) and scanning electron microscopy (SEM) observations reveal the formation of two or three elementary layers through the lattice exfoliation.

Introduction

There has been great interest in layered perovskite compounds because of their versatility in materials applications such as ferroelectrics, superconductors and ion conductors[1–3] as well as their structural anisotropy and unique intercalation behavior.[4] A series of layered perovskites, represented by the chemical formula of $A'[A_{n-1}B_nO_{3n+1}]$, has been extensively studied since $M^ICa_2Nb_3O_{10}$ (M^I = Li, Na, K$\cdots$) was prepared by Dion *et al.*[5] These Dion–Jacobson phases are composed of a number (*n*) of BO_6 (B = Nb^{5+}, Ta^{5+}, Ti^{4+},$\cdots$) octahedral slabs stacked along the (00*l*) direction and alkali metal cations (A′) between the layers. Recently, Ti- and Nb-based layered perovskites have become of great interest as active UV photocatalysts because they become semiconductors under band gap irradiation (E_g = 3.2–3.5 eV) to produce hole (h^+)–electron (e^-) pairs. The photoinduced hole–electron pairs subsequently take part in the photocatalytic reactions such as overall water splitting into H_2 and O_2, fixation of CO_2, photodegradation of hazardous organics, *etc.*[6]

From the viewpoint of photocatalysis, layered perovskites exhibit some unique characteristics. For example, layered perovskites possess exchangeable interlayer metal cations, which are easily replaced by foreign species to enhance or modify the photocatalytic activity. For instance, layered perovskite-type niobate, $KCa_2Nb_3O_{10}$, was found to exhibit high activity for photocatalytic H_2 evolution from an aqueous methanol solution after substitution of H^+ ions for alkali metal cations (K^+) in the interlayer space. Further modifications of interlayer spaces by loading of ultrafine Ni particles or pillaring of metal oxides have been also reported to improve the photocatalytic activity.[7] More significantly, the layered perovskite-type family has a lot of derivatives resulting from the replacement of the elements of perovskite slabs with other elements, providing an opportunity to fine-tune chemical and physical properties of the compounds by proper selection of the constituent elements. For example, $RbPb_2Nb_3O_{10}$, which is an analogue of $KCa_2Nb_3O_{10}$, has been found to show photocatalytic activity under irradiation by visible light (>420 nm).[8]

Another promising way of exploiting the interlayer spaces of layered metal oxides is the exfoliation of bulk oxide layers into their elementary layers by, so-called, soft-chemical processes. Chemical exfoliation of layered materials provides an efficient way of preparing nanocrystalline particles or colloidal solutions, which are versatile precursors in preparing thin films,[9] membranes, porous composites,[10] and layered nanocomposites.[11] Moreover, exfoliated nanolayers behave like a new kind of inorganic macromolecules, which differ markedly from their bulk counterparts in physical properties such as quantum-size effects.[12] Some inorganic layered solids, such as clay minerals, layered titanates, niobates, phosphates and superconductors, have been reported to be exfoliated in aqueous solutions containing amine surfactants.[9–11]

In general, exfoliation of layered metal oxides including layered perovskites can be achieved by treating the lamellar compounds with specific amine surfactants (*e.g.* TBA^+) under restricted conditions (*e.g.* ultrasonication[13]). However, only some of the lamellar crystals are successfully delaminated into individual nanolayers, mainly due to the poor swelling properties of the crystals.[14] Therefore an economic alternative is required to improve the productivity and reproducibility of the conventional exfoliation process.

Here, we describe a novel exfoliation process of lamellar metal oxides *via* amino acid intercalation compounds. Since amino acids are typical zwitterions with amine ($-NH_2$) and carboxylic (–COOH) functional groups within a molecule, it becomes cationic ($-NH_3^+$) in acid media, while anionic ($-COO^-$) in basic media. Thus, amino acid molecules can be easily intercalated between negatively charged metal oxide layers by simple cation exchange reaction with interlayer

DOI: 10.1039/b006045n

cations (K^+ or H^+) under acidic conditions. After being intercalated, increasing the solution pH *via* base titration would cause deprotonation of the –COOH groups of the interlayer amino acid molecules to form anionic $–COO^-$ terminal groups. Thus derived anionic $–COO^-$ groups may interact repulsively with the negatively charged metal oxide layers, forcing the metal oxide layers apart, eventually leading to infinite swelling, *i.e.* exfoliation of metal oxide layers into individual nanosheets. Because this novel process utilizes the electrostatic repulsive force between guest species and inorganic host layers, it is particularly suitable for the exfoliation of metal oxide layers with poor swelling properties due to their high layer charge density.

In the present study, primary attention is paid to the intercalation of long chain amino acid molecules into the perovskite slabs of $KCa_2Nb_3O_{10}$ to prepare precursor amino acid-layered perovskite compounds. Then the exfoliation of calcium niobate sheets into the elementary layers is carried out by simple base titration to verify the exfoliation process experimentally. Finally, the resulting nanoparticles and colloidal solution are systematically analyzed by XRD, thermogravimetric/differential thermal analysis (TG/DTA), IR, UV-Vis, AFM, SEM, and BET in detail.

Experimental

Materials

$KCa_2Nb_3O_{10}$ was prepared by firing a stoichiometric mixture of K_2CO_3 (Osaka, >99.5%), $CaCO_3$ (Aldrich, >99%), and Nb_2O_5 (Aldrich, 99.9%) at 800 °C for 12 h in air and subsequent annealing at 1200 °C for 12 h after regrinding. As-prepared $KCa_2Nb_3O_{10}$ was then converted into its protonated derivative by refluxing the powder (2 g) in 6 mol dm^{-3} HCl solution (100 mL) at room temperature for 48 h. After repeating the above process twice, the solid product was recovered by centrifugation, washed with distilled water thoroughly to remove excess acid and then dried in air. In order to exchange the protons between the perovskite layers with amino acid molecules, the H^+ derivative was reacted with an aqueous solution containing aminoundecanoic acid (AUA), $H_2N(CH_2)_{10}COOH$ (99%, Aldrich, 2.3 g). Prior to the exchange reaction, the pH of the aqueous amino acid solution was adjusted to *ca.* 3 by adding 0.1 mol dm^{-3} HCl solution to derive the cationic AUA species. The above ion exchange procedure was repeated twice for complete cation exchange. Then the separated AUA derivative was washed with acidic aqueous solution (pH *ca.* 3) thoroughly and finally dried at 60 °C in an oven.

Exfoliation

Exfoliation of calcium niobate layers was carried out by dispersing the AUA derivative (40 mg) into various basic solutions (NaOH, 20 mL) with initial pH values of 11, 11.5, and 12, respectively, and continuously stirring at room temperature for 12 h to promote the intralayer deprotonation of carboxylic (–COOH) groups of the interlayered amino acid molecules. As the exfoliation proceeded, the initial pH values of the suspension were gradually decreased to 8.2, 8.6, and 9.2 respectively, indicating the partial neutralization of base (OH^-) by the dissociated protons (H^+) from interlayer carboxylic acids. The experimental pH values for the exfoliation were determined from the zeta-potential measurement for the AUA derivative depending upon the solution pH (see below, Fig. 5) and the preliminary solubility test of AUA molecules. Thus estimated experimental pHs of 8–9 achieve the intralayer deprotonation of carboxylic acid (–COOH), and exfoliation of niobate layers also occurs in the similar range of pH > 8, where amino acids have the anionic carboxylate form ($–COO^-$). The suspensions were left for a further 12 h without stirring, and then some precipitates, formed during aging *via* a partial replacement of the AUA molecules on the exfoliated niobate layers with Na^+ ions, were removed by decantation to obtain colloidal suspensions of exfoliated calcium niobate nanoparticles. Thus-prepared colloidal suspensions were stable for at least 3 months without any precipitation. Some of the colloidal suspension prepared at the initial pH of 12 was separated and restacked by titrating with an aqueous 6 mol dm^{-3} HNO_3 solution, and then the resulting solid was recovered by centrifugation, washed with 6 mol dm^{-3} HNO_3, and finally dried at 100 °C in an oven.

Characterization

Powder X-ray diffraction (XRD) patterns were recorded on a Philips PW 3710 powder diffractometer equipped with Ni-filtered Cu-K_α radiation ($\lambda = 1.5418$ Å). For the X-ray diffraction measurement the K, H, and AUA derivatives and restacked calcium niobate samples were mounted on a glass sample holder. In the case of colloidal samples, the colloidal suspensions were spread on a glass slide and dried at room temperature to obtain thin films. Simultaneous thermogravimetric (TG) and differential thermal analyses (DTA) were performed using a Rigaku TAS-100 thermal analyzer. Samples were heated in the range 25–800 °C at a heating rate of 5 °C min^{-1} under a N_2–O_2 gas atmosphere ($N_2 : O_2 = 8 : 2$ by vol). Infrared (IR) spectra were recorded on a Bruker IFS-88 FT-IR spectrometer by the standard KBr disk method in the range 500–4000 cm^{-1} with a resolution of 2 cm^{-1}. A Perkin-Elmer Lambda 12 UV-vis spectrometer was used to obtain the absorption spectra of the pristine $HCa_2Nb_3O_{10}$ and colloidal suspensions prepared at various pHs by dispersing a weighed amount of solid sample (40 mg) in distilled water (20 mL). Electrokinetic potential (ζ-potential) diagrams as a function of solution pH were obtained using a Zetasizer 3000 (Malvern instruments) by titrating slowly 0.1 mol dm^{-3} NaOH solution to the aqueous suspension of the AUA derivative (200 mg; 100 mL). The value of the zeta potential was recorded after equilibrating the suspension for 2 h to achieve acid–base equilibrium. Atomic force microscope (AFM) images were obtained using a Digital Instruments Model Nanoscope IIIa scanning probe microscope with V-shaped and 200 μm long Si_3N_4 cantilevers (force constant = 0.12 N m^{-1}, Nanoscope Digital Instruments). The sample for AFM observation was prepared by diluting the suspension (0.05 mL) obtained at the initial pH = 12 with deionized water (5 L) and dropping the resulting suspension on a silicon wafer. The morphological evolution of calcium niobate during the exfoliation process was observed by scanning electron microscopy (SEM, Hitachi S-4500). Prior to the observation, all the samples were coated with Pt/Pd for 180 s by E-1030 ion sputtering (Hitachi). The nitrogen adsorption–desorption isotherms were measured volumetrically at liquid nitrogen temperature (−196 °C) with a computer-controlled measurement system. Samples were degassed at 200 °C for 2 h under reduced pressure ($<10^{-4}$ Torr) prior to sorption measurements. The specific surface areas for the samples were calculated by using the BET equation.

Results and discussion

Intercalation

Powder XRD patterns of the pristine $KCa_2Nb_3O_{10}$ and its proton (H^+) and AUA derivatives are shown in Fig. 1. The observed diffraction lines in $KCa_2Nb_3O_{10}$ (a) and $HCa_2Nb_3O_{10}$ (b) are indexed successfully on the basis of a tetragonal unit cell with $a/2 = 3.86$ Å, $c/2 = 14.8$ Å, and $a = 3.85$ Å, $c = 14.4$ Å, respectively, which are in good agreement with the literature

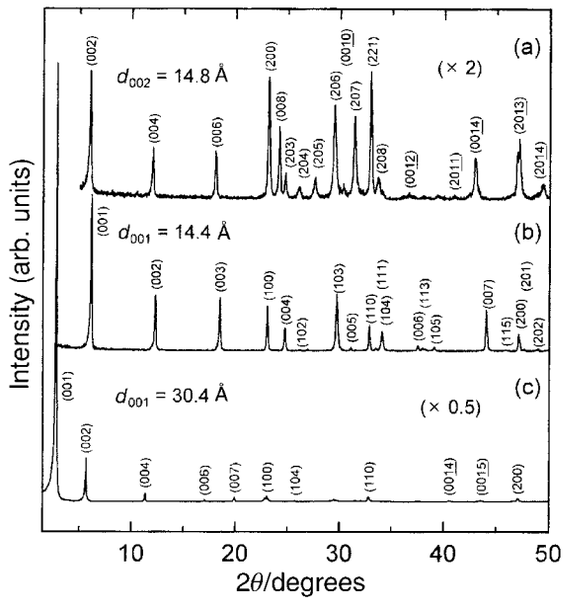

Fig. 1 Powder XRD patterns for (a) $KCa_2Nb_3O_{10}$, (b) $HCa_2Nb_3O_{10}$, and (c) the AUA derivative, respectively. The intensities of (a) and (c) were multiplied by 2 and 0.5 for ease of comparison.

values.[5] Reaction of $HCa_2Nb_3O_{10}$ with 11-aminoundecanoic acid (AUA) leads to an AUA intercalated calcium niobate with a basal spacing of 30.4 Å (c). Assuming that the basal spacing of $HCa_2Nb_3O_{10}$ is ~14.4 Å,[15] the gallery height due to the AUA pillaring is estimated to be 16.0 Å. Taking into account the theoretical molecular length of AUA (18.5 Å),[16] the interlayer AUA molecules are expected to have a paraffin-like monolayer structure with a tilt angle of *ca.* 61° to the oxide layers.

TG and DTA curves for the AUA derivative are represented in Fig. 2. At first, the weight loss below 200 °C with weak endothermic peaks in the DTA curve can be ascribed to the evaporation of surface adsorbed or some interlayer water. Secondly, the drastic mass loss accompanied by a sharp exothermic effect in the DTA curve at around 320 °C is mainly due to the oxidative decomposition of interlayer AUA molecules. An additional weight loss observed above 550 °C can be assigned to the decomposition of residual carbonaceous compounds formed during the pyrolysis of AUA molecules. The total weight loss owing to the decomposition of AUA molecules is estimated to be 15.1% from the mass loss occurring in the temperature range 200–800 °C.

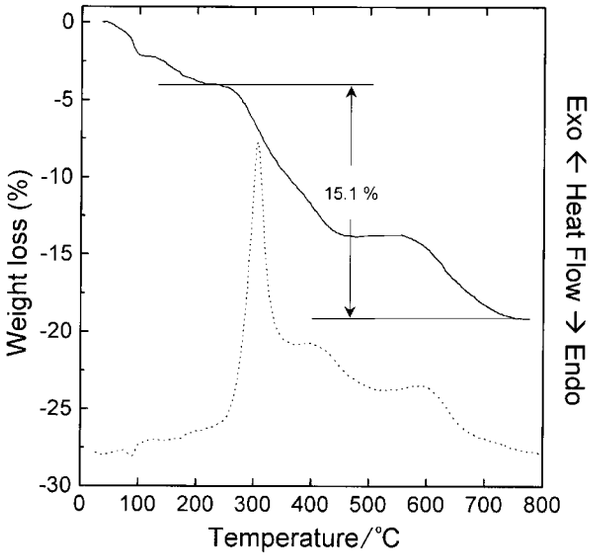

Fig. 2 Simultaneous TG and DTA curves for the AUA derivative.

On the basis of TG analysis, the chemical formula of the AUA derivative is proposed to be $H_{0.5}(AUA)_{0.5}Ca_2Nb_3O_{10}$, indicating that only half of the interlayer protons are replaced by AUA molecules. Neither prolonged treatment nor high temperature reactions drove the reaction beyond this loading level. Such an incomplete replacement of the interlayer protons by AUA is primarily due to strong steric hindrance. Since the van der Waals radius of the methyl group is 2.0 Å, and the chains cannot come into close contact with each other (less than 1.65 Å),[17] the cross-sectional area of an intercalated AUA molecule is about 25.1 Å^2 ((2.0 Å + 1.65 Å)$^2\pi$). The available unit surface area of ($Ca_2Nb_3O_{10}^-$) is 14.8 Å^2 ($a \times b$, $a = b = 3.85$ Å), implying that only half of the AUA molecules can be accommodated in the unit area of ($Ca_2Nb_3O_{10}^-$). Therefore, the residual protons would occupy vacant sites in the basal plane, compensating the excess negative layer charge. Note that the steric restriction is not solely responsible for the incomplete ion exchange. As is well demonstrated in the case of amine intercalation into metal oxide layers,[17,18] the interlayer amines tend to form paraffin-type bilayers to overcome such steric restrictions. A clue to the extra stabilization of the monolayer arrangement of interlayered amino acid molecules between perovskite layers can be obtained from the following infrared absorption spectroscopic analysis.

Fig. 3 shows the Fourier transformed IR spectra of AUA (zwitterionic species; $NH_3^+(CH_2)_{10}COO^-$) (a), $HCa_2Nb_3O_{10}$ (b), and AUA-intercalated calcium niobate (c). Absorption peaks appearing at 596 and 779 cm^{-1} are assigned to the characteristic internal Nb–O vibrational modes in the NbO_6 octahedron[19] and the sharp absorption pair at 2852 and 2924 cm^{-1} correspond to aliphatic C–H stretching bands of AUA. The absorption band at 1643 cm^{-1} in Fig. 3(a) is assigned to the antisymmetric stretching vibration ($\nu_{asC=O}$) of carboxylates in free AUA molecules, suggesting the formation of an intermolecular complex as graphically depicted in the figure. The $\nu_{C=O}$ of interlayered AUA appears at 1707 cm^{-1} (Fig. 3(c)), implying the presence of un-ionized –COOH groups (*cf.* $\nu_{C=O}$ of free carboxylic acid monomer is *ca.* 1760 cm^{-1}).[20] The red shift of $\nu_{C=O}$ in the interlayered AUA compared to that of free AUA can be ascribed to the formation of intermolecular hydrogen bonding.[20] As schematically shown in the inset, the

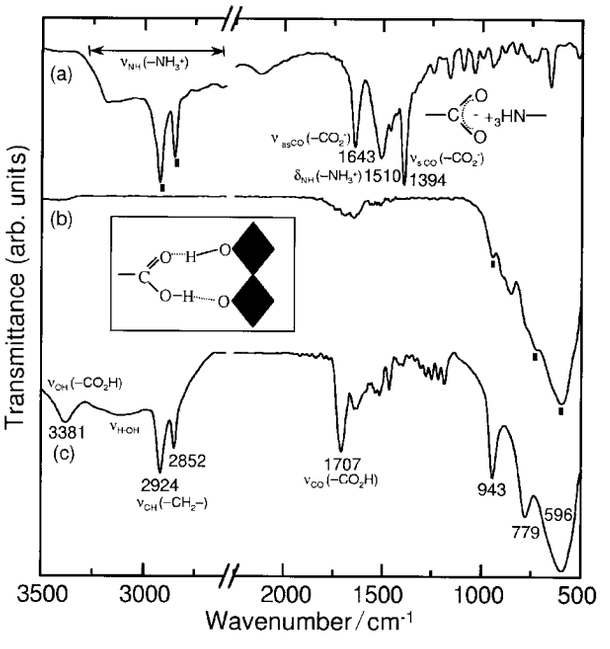

Fig. 3 Fourier transformed infrared spectra (FT-IR) for (a) AUA only, (b) $HCa_2Nb_3O_{10}$, and (c) the AUA derivative.

terminal –COOH groups in the interlayer AUA molecules are directed toward the oxygen plane of the perovskite layers to form hydrogen bonds, leading to the extra stabilization of the monolayer arrangement of interlayer AUA molecules between perovskite layers.

Exfoliation

The evolution of X-ray diffraction (XRD) patterns upon exfoliation at different initial suspension pHs is represented in Fig. 4. As can be seen, the intensities of the (00*l*) reflections gradually diminish with increasing pH, and mostly disappear at the initial pH = 12 (final pH = 9.2) (d), indicating the disappearance of long-range ordered layer stacking due to the delamination of oxide layers into individual nanosheets. Since the carboxylic group of the intercalated amino acid molecules becomes deprotonated in basic solution, an electrostatic repulsion between anionic carboxyl groups ($^{+}NH_3(CH_2)_{10}COO^{-}$) and negatively charged oxide layers ($Ca_2Nb_3O_{10}^{-}$) would occur, consequently leading to the delamination of metal oxide layers into elementary nanosheets in aqueous solution.

When the exfoliated colloidal suspensions are titrated with aqueous HNO_3 solution, individual calcium niobate sheets are reassembled through the surface ion exchange reaction between AUA molecules and protons. The X-ray diffraction profile for the restacked product is shown in the inset of Fig. 4. The (001) reflection observed at $2\theta = 5.9°$ ($d_{001} = 15.0$ Å) is approximately consistent with that of $HCa_2Nb_3O_{10}$ ($2\theta = 6.1°$, $d_{001} = 14.4$ Å, Fig. 1(b)). Even though the line width of the diffraction profile is quite broad due to the lack of coherent layer stacking, this result strongly suggests that the two-dimensional character of the metal oxide layers is retained even after complete layer exfoliation.

The electrokinetic potential (ζ potential) of the suspension was measured as a function of pH to probe the surface charge variation during the exfoliation process (Fig. 5). The negative zeta potential remains constant at least up to pH 8, becoming more negative at a rapid rate with increasing solution pH. It is therefore presumed that the base titration causes the intralayer deprotonation of carboxylic groups, and consequently facilitates the delamination of oxide layers into individual niobate sheets where the amino acid molecules are anchored with the terminal $–COO^{-}$ groups exposed to the surrounding liquid.

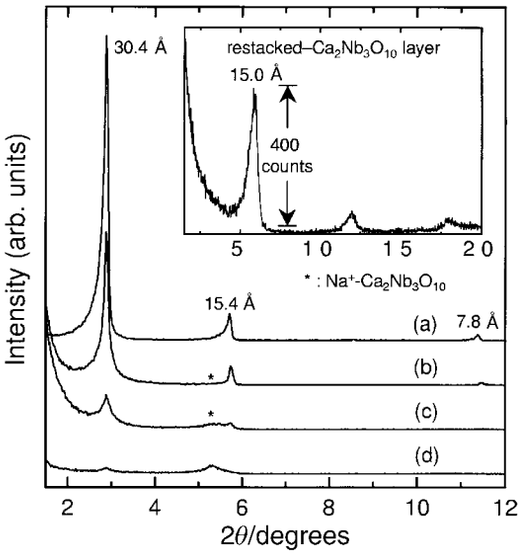

Fig. 4 Powder X-ray diffraction patterns. (a) AUA-intercalated $Ca_2Nb_3O_{10}$, (b)–(d) exfoliated samples in basic suspensions with initial pHs of 11, 11.5, and 12, respectively. X-Ray pattern of the restacked $HCa_2Nb_3O_{10}$ is also compared in the inset.

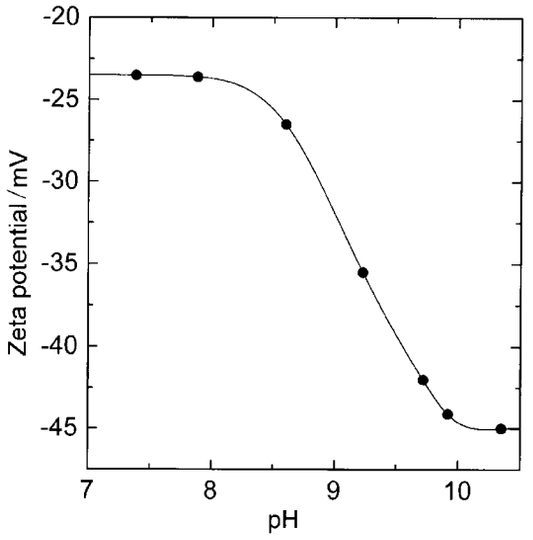

Fig. 5 Zeta potential diagram of the AUA derivative suspension as a function of pH in aqueous solution.

Thus, the increase of the negative zeta potential with pH reflects the increase of the proportion of exfoliated oxide layers.

Fig. 6 compares the UV-vis absorption spectra for the parent $HCa_2Nb_3O_{10}$ and its colloidal suspension obtained at the given initial pHs. At first, the absorption curves for colloidal nanosheets show a large spectral blue shift compared to that of the parent compound, which is mainly attributable to the size quantization effect[12] owing to the layer exfoliation. The band gap energies estimated from the absorption onset are 3.33 eV for the parent $HCa_2Nb_3O_{10}$ and 3.45 eV for the exfoliated one, respectively. As shown in the figure, the optical absorbance of the colloidal solutions increases linearly with the suspension pH, suggesting that the exfoliation becomes more favorable as the suspension pH increases due to rapid deprotonation of –COOH groups.

Further evidence on the exfoliation of perovskite layers into elementary nanosheets can be deduced from AFM analysis. Fig. 7(a) and (b) show the AFM image and corresponding height profile, respectively, for the sample obtained at the initial pH of 12. As can be seen, the apparent size of the

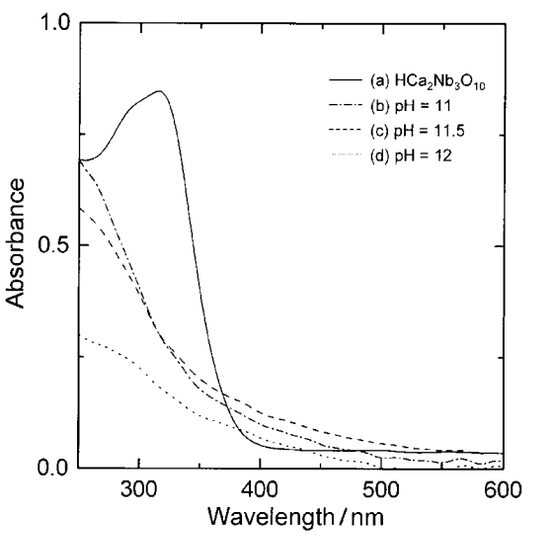

Fig. 6 UV-vis absorption spectra for the pristine $HCa_2Nb_3O_{10}$ powder (a) and colloidal suspensions obtained at the initial pH of (b) 11, (c) 11.5 and (d) 12, respectively. The pristine $HCa_2Nb_3O_{10}$ powder was measured in the reflection mode while the colloidal solutions were measured in transmission mode due to their differing dispersion properties.

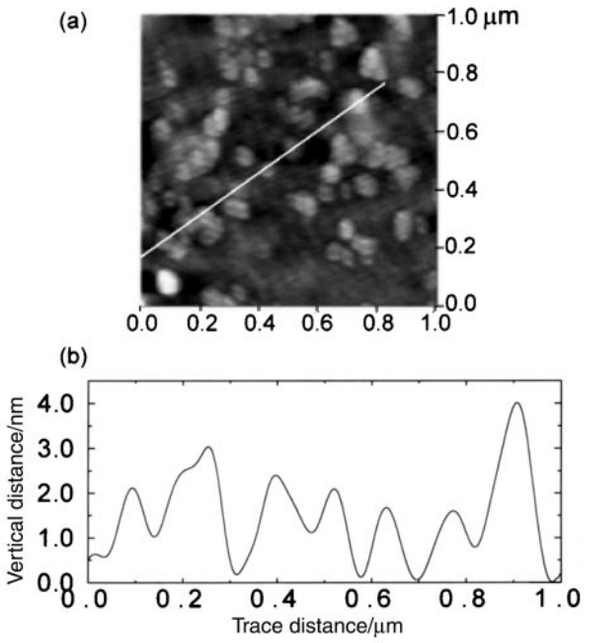

Fig. 7 AFM image (a) and section profile (b) of the exfoliated calcium niobate particles prepared at the initial pH = 12.

particles falls into the range 100–200 nm in lateral dimension and 1.4–4.2 nm in height. Assuming that the average basal spacing is ~1.4 nm, it is found that the exfoliated particles consist of 1–3 elementary oxide sheets. Along with the delamination of oxide layers in the *c*-direction, the fragmentation of large oxide plates into finely divided ones (100–200 nm) in the lateral direction seems to occur simultaneously due to the layer deformation in the course of AUA intercalation and/or exfoliation.

The morphological evolution upon exfoliation is also monitored by SEM (Fig. 8). The parent microcrystals with lamellar structure (a) become disintegrated into thinner layers consisting of a few hundred elementary oxide sheets (b, initial pH = 11.0). As the initial pH of the suspension increases to 11.5 (c), the oxide layers are further finely divided, and eventually form exfoliated oxide layers consisting of several oxide nanosheets (d, initial pH = 11.5).

The particle textures of the pristine $HCa_2Nb_3O_{10}$ and the exfoliated-restacked $HCa_2Nb_3O_{10}$ are deduced from the

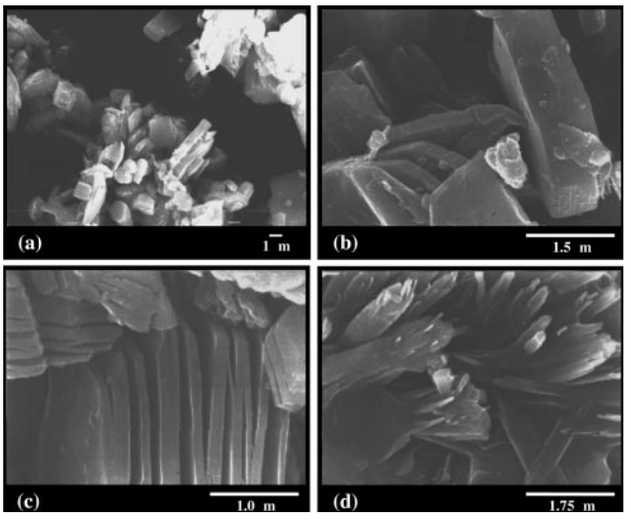

Fig. 8 Morphological evolution of calcium niobate particles upon exfoliation observed by SEM. (a) AUA-intercalated $Ca_2Nb_3O_{10}$, and (b)–(d) the exfoliated calcium niobate particles prepared at the initial pH of 11, 11.5, and 12, respectively.

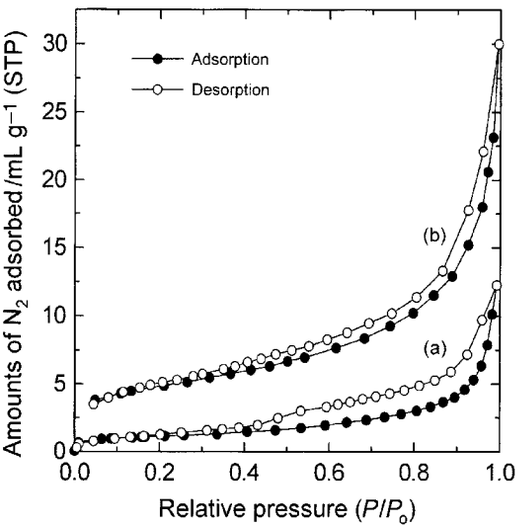

Fig. 9 Nitrogen adsorption–desorption isotherms of the pristine $HCa_2Nb_3O_{10}$ (a) and restacked $HCa_2Nb_3O_{10}$ (b). The samples were degassed at 200 °C for 2 h prior to the sorption measurements.

nitrogen absorption–desorption isotherms (Fig. 9). The adsorption isotherm of pristine $HCa_2Nb_3O_{10}$ (a) follows type II in the BDDT classification,[21] which is indicative of N_2 adsorption on non-porous materials. The BET specific surface area is calculated to be $S_{BET} = \sim 2\ m^2\ g^{-1}$. The restacked $HCa_2Nb_3O_{10}$ (b) exhibits largely enhanced N_2 adsorption capacity with $S_{BET} = \sim 16\ m^2\ g^{-1}$. This result suggests that the exfoliated particles are piled up rather loosely and irregularly during restacking to create many voids between the exfoliated particles.

Conclusion

Protonic layered perovskite ($HCa_2Nb_3O_{10}$) is successfully exfoliated into elementary oxide nanosheets *via* an amino-undecanoic acid (AUA) intermediate utilising a host–guest repulsive intercalation induced by deprotonation of the carboxylic groups in the interlayered amino acid molecules with NaOH titration. The exfoliated oxide nanoparticles show excellent colloidal stability in an aqueous solution with remarkable blue shifts in UV absorption spectra depending upon the pH conditions due to the size quantization effect. Microscopic observations also confirm the delamination of the pristine lamellar material into the oxide nanosheets.

Acknowledgements

This work was supported by Ministry of Science and Technology (MOST) through the National Nanohybrid Materials Laboratory of NRL Project '99 and partially by the Brain Korea 21 program–LG Electronics Institute of Technology.

References

1 R. Ramesh, A. Inam, W. K. Chan, B. Wilkens, K. Myers, K. Remsching, D. L. Hart and J. M. Tarascon, *Science*, 1991, **252**, 944; C. B. Eom, R. J. Cava, R. M. Fleming, J. M. Phillips, R. B. Van Dover, J. H. Marshall, J. W. P. Hsu, J. J. Krajewski and W. F. Peck, *Science*, 1992, **258**, 1766; C. A. Paz de Araujo, J. D. Cuchiaro, L. D. McMillan, M. C. Scott and J. F. Scott, *Nature*, 1995, **374**, 627.

2 A. W. Sleight, *Science*, 1988, **242**, 1519; R. J. Cava, *Science*, 1990, **247**, 656; R. J. Cava, *Science*, 1990, **247**, 656; J. G. Bednorz and K. A. Müller, *Z. Phys. B*, 1986, **64**, 189.

3 Y. Inaguma, L. Chen, M. Itoh and T. Nakamura, *Solid State Ionics*, 1994, **70/71**, 196.

4 A. J. Jacobson, J. W. Johnson and J. T. Levandowski, *Inorg. Chem.*, 1985, **24**, 3727; A. J. Jacobson, J. W. Johnson and J. T. Levandowski, *Mater. Res. Bull.*, 1987, **22**, 45; S. Uma and J. Gopalakrishnan, *J. Mater. Sci. Eng. B*, 1995, **34**, 175; T. Nakato, K. Kusunoki, K. Yoshizawa, K. Kuroda and M. Kaneko, *J. Phys. Chem.*, 1995, **99**, 17896; J. H. Choy, S. J. Kwon and G. S. Park, *Science*, 1998, **280**, 1589.
5 M. Dion and M. Ganne, *Mater. Res. Bull.*, 1981, **16**, 1429.
6 K. Domen, A. Kudo, A. Shinozaki, K. Maruya and T. Onishi, *J. Chem. Soc., Chem. Commun.*, 1986, 356; K. Sayama, K. Tanaka, K. Domen, K. Maruya and T. Onishi, *J. Phys. Chem.*, 1991, **59**, 1345; M. Ogawa and K. Kuroda, *Chem. Rev.*, 1995, **95**, 399; S. Uchida, Y. Yamamoto, Y. Fujishiro, A. Watanabe and O. Ito, *J. Chem. Soc., Faraday Trans.*, 1997, **93**, 3229; S. Ikeda, M. Hara, J. N. Kondo, K. Domen, H. Takahashi, T. Okubo and M. Kakihana, *Chem. Mater.*, 1998, **10**, 72; T. Takata, A. Tanaka, M. Hara, J. N. Kondo and K. Domen, *Catal. Today*, 1998, **44**, 17.
7 K. Domen, A. Kudo and T. Onishi, *J. Catal.*, 1986, **102**, 92; A. Kudo, K. Domen, K. Maruya and T. Onishi, *Chem. Phys. Lett.*, 1987, **133**, 517; A. Kudo, A. Tanaka, K. Domen, K. Maruya, K. Aika and T. Onishi, *J. Catal.*, 1988, **111**, 67; K. Sayama, A. Tanaka, K. Domen, K. Maruya and T. Onishi, *J. Catal.*, 1990, **142**, 541; K. Sayama, H. Arakawa and K. Domen, *Catal. Today*, 1996, **28**, 175; K. Sayama, H. Arakawa and K. Domen, *Catal. Today*, 1996, **28**, 175; R. Abe, K. Shinohara, A. Tanaka, M. Hara, J. N. Kondo and K. Domen, *Catal. Today*, 1997, **9**, 2179.
8 J. Yoshimura, Y. Ebina, J. Kondo, K. Domen and A. Tanaka, *J. Phys. Chem.*, 1993, **97**, 1970.
9 T. J. Pinnavaia, *Science*, 1983, **220**, 365; Z. Wang and T. J. Pinnavaia, *Chem. Mater.*, 1998, **10**, 1820; A. Corma, V. Fornes, S. B. Pergher, T. L. M. Maeesen and J. G. Buglass, *Nature*, 1998, **396**, 353; T. Sasaki and M. Watanabe, *J. Phys. Chem. B*, 1997, **101**, 10159; T. Sasaki and M. Watanabe, *J. Am. Chem. Soc.*, 1998, **120**, 4682; G. Alberti, M. Casciola and U. Costantino, *J. Colloid Interface Sci.*, 1985, **107**, 256; G. Alberti and F. Marmottini, *J. Colloid Interface Sci.*, 1993, **157**, 513; G. Alberti, M. Casciola, U. Costantino, A. Peraio and T. Rega, *J. Mater. Chem.*, 1995, **5**, 1809; J. H. Choy, S. J. Kwon, S. J. Hwang, Y. I. Kim and W. Lee, *J. Mater. Chem.*, 1999, **9**, 129; R. Abe, M. Hara, J. N. Kondo and K. Domen, *Chem. Mater.*, 1998, **10**, 1647.
10 F. Kooli, T. Sasaki and M. Watanabe, *Chem. Commun.*, 1999, 211.
11 E. R. Kleinfeld and G. S. Ferguson, *Science*, 1994, **265**, 370; D. M. Kaschak, S. A. Johnson, D. E. Hooks, H. N. Kim, M. D. Ward and T. E. Mallouk, *J. Am. Chem. Soc.*, 1998, **120**, 10887.
12 A. Henglein, *Chem. Rev.*, 1989, **89**, 1861.
13 M. M. J. Treacy, M. E. Bisher and A. Jacobson, *Philos. Mag. A*, 1995, **72**, 161; S. Sivakumar, A. D. Damodaran and K. G. K. Warrier, *Ceram. Inter.*, 1995, **21**, 85.
14 Y. Ebina, A. Tanaka, J. N. Kondo and K. Domen, *Chem. Mater.*, 1996, **8**, 2534; K. Domen, Y. Ebina, S. Ikeda, A. Tanaka, J. N. Kondo and K. Maruya, *Catal. Today*, 1996, **28**, 167.
15 A. J. Jacobson, J. T. Levandowski and J. W. Johnson, *J. Less Comm Met.*, 1986, **116**, 137.
16 A. Usuki, M. Kawasumi, Y. Kojima, A. Okada, T. Kurauchi and O. Kamigaito, *J. Mater. Res.*, 1993, **8**, 1174.
17 J. F. Lambert, Z. Deng, J. B. D'espinose and J. J. Fripiat, *J. Colloid Interface Sci.*, 1989, **132**, 337.
18 A. Grandin, M. M. Borel and B. Raveau, *J. Solid State Chem.*, 1985, **60**, 366.
19 G. Blasse and A. F. Corsmit, *J. Solid State Chem.*, 1973, **6**, 513.
20 R. M. Silverstein, G. C. Bassler and T. C. Morrill, in *Spectrometric Identification of Organic Compounds*, John Wiley & Sons, New York, 1991, pp. 117–118.
21 S. J. Gregg and K. S. W. Sing, in *Adsorption, Surface Area and Porosity*, Academic Press, London, 1982.